Simulations of Relativistic Astrophysical Flows

J. Bergmans[1], R. Keppens[2], D.E.A. van Odyck[3], A. Achterberg[1]

[1] Sterrenkundig Instituut, Utrecht
[2] Instituut voor Plasmafysica "Rijnhuizen", Nieuwegein
[3] Centrum voor Wiskunde en Informatica, Amsterdam

The multidimensional grid-adaptive magnetofluid dynamics code AMRVAC [1, 2] has been extended with special relativistic hydrodynamics and magnetohydrodynamics modules to simulate the complex and ultra-relativistic flow dynamics associated with astrophysical objects like Gamma Ray Bursts and Active Galactic Nuclei. The shock capturing numerical scheme and mesh refinement algorithm are crucial to resolve the strong shocks and wide range of length scales present in these flows.

The first results look promising, we can simulate strongly relativistic blast waves, fireballs, and jets in 1D, 2D, and 3D.

1 Introduction

Relativistic flows are directly observed, or indirectly inferred, in a variety of astrophysical objects. Accretion flows and collimated jets around massive black holes in Active Galactic Nuclei have Lorentz factors of order 10, which means velocities of 99.5% of the speed of light (the Lorentz factor is defined as $\Gamma = (1 - v^2/c^2)^{-1/2}$). Even stronger relativistic flows are presumed to be the origin of Gamma Ray Bursts, the most energetic events in the observable universe since the Big Bang. Energy and time scales suggest that the source must be accompanied by an extremely relativistic explosion or jet flow with Lorentz factors in the order of 10^2 to 10^3, almost certainly also in the form of a collimated jet. Strong shocks and magnetic fields are responsible for the production of high-energy particles and radiation from these systems.

Numerical simulations of the dynamical interplay between relativistic flow, strong shocks and magnetic fields are valuable to describe and understand the observed properties of relativistic astrophysical objects. The calculation will have to be capable of resolving the large-scale flows and at the same time accurately capture the small-scale dynamics and shocks. This wide range of dynamical length scales makes it necessary to employ adaptive mesh refinement techniques.

Because the flows under consideration are in general on a much larger scale than the size of the central compact object, it is in first approximation reasonable to describe the system in flat space-time, i.e. using the special relativistic incarnation of ideal (magneto-)hydrodynamics. The governing equations are given in Sec. 2. In Sec. 3 we describe the numerical code AMRVAC which has been extended with relativistic HD and MHD physics modules. In Sec. 4 some test problems and results for both relativistic HD and MHD calculations are shown.

2 Equations for Relativistic Fluids

The fluid equations follow from particle conservation, the conservation of the energy-momentum tensor, and an induction equation for the magnetic field. The continuity equation (in units where $c = 1$, Greek indices denote four-vectors and Latin indices denote three-vectors) is given by

$$\partial_\alpha(\rho u^\alpha) = 0 \; , \tag{1}$$

where ρ is the rest mass density, $u^\alpha = \Gamma(1, \boldsymbol{v})$ is the four-velocity for which $u_\alpha u^\alpha = -1$, and the Lorentz factor is $\Gamma = (1 - v^2)^{-1/2}$.

The second ingredient is the conservation of the stress-energy tensor

$$\partial_\alpha(T^{\alpha\beta}_{\mathrm{fl}} + T^{\alpha\beta}_{\mathrm{em}}) = 0 \; . \tag{2}$$

For pure hydrodynamics the electromagnetic part is absent, so for an ideal fluid the stress-energy tensor is given by (See [3])

$$T^{\alpha\beta} = T^{\alpha\beta}_{\mathrm{fl}} = w u^\alpha u^\beta + p\eta^{\alpha\beta} \; . \tag{3}$$

The relativistic enthalpy is $w = e + p$, where the energy per unit volume e includes the rest mass energy, and p is the kinetic pressure. The Minkowski metric tensor is $\eta^{\alpha\beta} = \mathrm{diag}\{-1, 1, 1, 1\}$. All thermodynamic quantities (ρ, p, e, w) are measured in the rest frame of the fluid. To close the system of equations we need an equation of state relating the kinetic pressure with density and internal energy, in this work we take a polytropic gas law with adiabatic index γ, for which the enthalpy is given by

$$w = \rho + \frac{\gamma}{\gamma - 1} p \; . \tag{4}$$

For real-world applications we separate the temporal from the spatial components and the equations of special relativistic hydrodynamics (from here onwards abbreviated as RHD) read

$$\partial_t(\Gamma\rho) + \partial_i(\Gamma\rho v^i) = 0 \; , \tag{5}$$

$$\partial_t(\Gamma^2 w v^j) + \partial_i(\Gamma^2 w v^i v^j + p\delta^{ij}) = 0 \; , \tag{6}$$

$$\partial_t(\Gamma^2 w - p) + \partial_i(\Gamma^2 w v^i) = 0 \; . \tag{7}$$

To arrive at a set of equations describing a relativistic *magneto*fluid (special relativistic magnetohydrodynamics or RMHD) we need to add the electromagnetic part $T^{\alpha\beta}_{\mathrm{em}}$ to the momentum-energy tensor and add an equation for the electromagnetic field. Using the field tensor $F^{\alpha\beta}$ ($F^{\alpha\beta} = -F^{\beta\alpha}$, $E_i = F^{0i}$ and $B_i = \frac{1}{2}\epsilon^{ijk}F^{jk}$) and its dual $\mathcal{F}^{\alpha\beta} = \frac{1}{2}\epsilon^{\alpha\beta\gamma\delta}F_{\gamma\delta}$ the Maxwell equations in covariant form are

$$\partial_\alpha F^{\alpha\beta} = -j^\beta \ , \qquad \partial_\alpha \mathcal{F}^{\alpha\beta} = 0 \ . \tag{8}$$

The inhomogeneous equation is used to calculate the four-current j^α. The current density in RMHD is given by $\boldsymbol{J} = \nabla \times \boldsymbol{B} - \partial_t \boldsymbol{E}$. The homogeneous equation comprises both the induction equation and $\nabla \cdot \boldsymbol{B} = 0$. The electromagnetic contribution to the momentum-energy tensor is given by

$$T^{\alpha\beta}_{\mathrm{em}} = F^{\alpha}{}_{\gamma}F^{\gamma\beta} + \tfrac{1}{4}\eta^{\alpha\beta}F_{\gamma\delta}F^{\gamma\delta} \ . \tag{9}$$

Ohm's law for a perfectly conducting fluid ($\boldsymbol{E} + \boldsymbol{v} \times \boldsymbol{B} = 0$) is written covariantly as

$$F^{\alpha\beta}u_\beta = 0 \ . \tag{10}$$

This expression can be used to eliminate $\boldsymbol{E}$ from the equations. This is done by introducing the four-vector $b^\alpha \equiv \mathcal{F}^{\alpha\beta}u_\beta$. The field tensor can then be written in the form $F^{\gamma\delta} = \epsilon^{\alpha\beta\gamma\delta}b_\alpha u_\beta$ The components of this new vector are given by

$$b^\alpha = [\Gamma(\boldsymbol{v}\cdot\boldsymbol{B}), \boldsymbol{B}/\Gamma + \Gamma(\boldsymbol{v}\cdot\boldsymbol{B})\boldsymbol{v}] \ , \tag{11}$$

and we can write the momentum-energy tensor (9) in the following form (note that $b^\alpha u_\alpha = 0$ and that $|b|^2 = b^\alpha b_\alpha = (\boldsymbol{v}\cdot\boldsymbol{B})^2 + \boldsymbol{B}^2/\Gamma^2$)

$$T^{\alpha\beta}_{\mathrm{em}} = |b|^2\left(u^\alpha u^\beta + \tfrac{1}{2}\eta^{\alpha\beta}\right) - b^\alpha b^\beta \ . \tag{12}$$

The energy-momentum conservation equation (2) takes the form

$$\partial_\alpha[w_{\mathrm{tot}}u^\alpha u^\beta - b^\alpha b^\beta + p_{\mathrm{tot}}\eta^{\alpha\beta}] = 0 \ , \tag{13}$$

where $w_{\mathrm{tot}} = w + |b|^2$ and $p_{\mathrm{tot}} = p + \frac{1}{2}|b|^2$. The induction equation from (8) transforms to

$$\partial_\alpha(u^\alpha b^\beta - b^\alpha u^\beta) = 0 \ . \tag{14}$$

The set of RMHD equations is composed of the continuity equation (1), the temporal and spatial parts of the momentum-energy equation (13), and the field equation (14). Again we split these equations in their temporal and spatial parts to obtain

$$\partial_t(\Gamma\rho) + \partial_i(\Gamma\rho v^i) = 0 \ , \tag{15}$$

$$\partial_t\left(\Gamma^2 w_{\mathrm{tot}} v^j - b^0 b^j\right) + \partial_i\left(\Gamma^2 w_{\mathrm{tot}} v^i v^j - b^i b^j + p_{\mathrm{tot}}\delta^{ij}\right) = 0 \ , \tag{16}$$

$$\partial_t\left(\Gamma^2 w_{\mathrm{tot}} - (b^0)^2 - p_{\mathrm{tot}}\right) + \partial_i\left(\Gamma^2 w_{\mathrm{tot}} v^i - b^0 b^i\right) = 0 \ , \tag{17}$$

$$\partial_t B^j + \partial_i\left(v^i B^j - B^i v^j\right) = 0 \ , \qquad \partial_i B^i = 0 \ . \tag{18}$$

The RHD equations (5)–(7) may be obtained from these equations simply by taking $\boldsymbol{B} = 0$; the non-relativistic MHD equations emerge in the limit $v^2 \ll 1$. When taking this limit one needs to subtract the contribution of the rest-mass energy density from the energy equation. The fact that the magnetic field equations are unchanged from classical MHD is of course due to the fact that Maxwell's equations are already Lorentz invariant.

2.1 Recovering the Primitive Variables

Although (15)–(18) are already in conservation form, we will rewrite them in the form actually used in the code:

$$\partial_t \boldsymbol{U} + \sum_i \partial_i \boldsymbol{F}^i = 0 \ , \tag{19}$$

where $\boldsymbol{U} = [D, \boldsymbol{S}, E, \boldsymbol{B}]^T$ with $D \equiv \Gamma\rho$, $\boldsymbol{S} \equiv (\Gamma^2 w + B^2)\boldsymbol{v} - (\boldsymbol{v}\cdot\boldsymbol{B})\boldsymbol{B}$ and $E \equiv \Gamma^2 w + B^2 - p_{\mathrm{tot}}$ are the conserved variables. The fluxes are given by $\boldsymbol{F}^i = \boldsymbol{U}v^i + [0, -\left(\boldsymbol{B}/\Gamma^2 + (\boldsymbol{v}\cdot\boldsymbol{B})\boldsymbol{v}\right) B^i + p_{\mathrm{tot}}\boldsymbol{I}^i, p_{\mathrm{tot}}v^i - (\boldsymbol{v}\cdot\boldsymbol{B})B^i, -\boldsymbol{v}B^i]^T$. $\boldsymbol{I}^i$ denotes the ith column of the identity matrix.

To numerically advance the conserved variables $(D, \boldsymbol{S}, E, \boldsymbol{B})$ in time one needs to calculate the values of the primitive variables $(\rho, \boldsymbol{v}, p, \boldsymbol{B})$ in order to determine the fluxes. In classical (M)HD this is an almost trivial operation, but due to the coupling between variables by various powers of the Lorentz factor we have to compute the primitive variables by numerically solving a nonlinear equation.

Following the method outlined in [4] we reduce the problem to an equation for $\xi \equiv \Gamma^2 w$, which is then solved by the Newton–Raphson method. First note that from the definition of $\boldsymbol{S}$ follows that $\boldsymbol{v}\cdot\boldsymbol{B} = \xi^{-1}\boldsymbol{S}\cdot\boldsymbol{B}$ and the velocity can be expressed in conserved variables and ξ only:

$$\boldsymbol{v} = \left(\boldsymbol{S} + \xi^{-1}(\boldsymbol{S}\cdot\boldsymbol{B})\boldsymbol{B}\right)/(\xi + B^2) \ . \tag{20}$$

Using the equation of state (4), the density and kinetic pressure are

$$\rho = D/\Gamma, \qquad p = (\gamma - 1)\left(\xi/\Gamma^2 - D/\Gamma\right)/\gamma \ . \tag{21}$$

From the definition of the total energy E we find a single equation for ξ:

$$f(\xi) = \xi - \frac{\gamma - 1}{\gamma}\left(\frac{\xi}{\Gamma^2} - \frac{D}{\Gamma}\right) + B^2 - \tfrac{1}{2}\left[\frac{B^2}{\Gamma^2} + \frac{(\boldsymbol{S}\cdot\boldsymbol{B})^2}{\xi^2}\right] - E = 0 \ , \tag{22}$$

where the Lorentz factor is given by

$$1/\Gamma^2 = 1 - \left(\boldsymbol{S} + \xi^{-1}(\boldsymbol{S}\cdot\boldsymbol{B})\boldsymbol{B}\right)^2/(\xi + B^2)^2 \ . \tag{23}$$

Given a set of values for the conserved variables $(D, \boldsymbol{S}, E, \boldsymbol{B})$ (22) is solved by means of the Newton–Raphson method. By (20) and (21) the complete set of primitive variables is then determined.

From (23) we see that $\Gamma^2 \geq 1$ and thus $v^2 < 1$, as required. The positivity of the density directly leads to the positivity of D. The condition $p > 0$ translates into the condition

$$\xi^2/\Gamma^2 > D^2 \ . \tag{24}$$

This condition is satisfied for $\xi > \xi_0$, where ξ_0 is the maximum root of the fourth order equation $\xi_0^2/\Gamma^2 = D^2$. Because $f(\xi)$ is a monotonically increasing function of ξ, we find that if $f(\xi_0) < 0$ then (22) has a single solution representing a physically allowable state.

2.2 Calculating Propagation Speeds

The numerical fluxes for the TVDLF method used in this work are based on the maximum propagation speed for a given state (see section 3). As the equations themselves are formulated in the observers frame, the propagation speeds are measured in that same frame. Although at the moment we need only the largest eigenvalue for our numerical scheme, in the future one might want to implement more sophisticated solvers based on more or all characteristic speeds, so for completeness we summarize all waves. For details we refer to [5, 4, 6] and references therein.

The system of RMHD equations admits seven waves: two Alfvén, two fast and two slow magnetosonic waves and one entropy wave. In contrast to classical MHD the symmetry of the wave speeds with respect to the fluid velocity is lost, but the ordering is still maintained: $\lambda_F^-, \lambda_A^-, \lambda_S^-, \lambda_0, \lambda_S^+, \lambda_A^+, \lambda_F^+$. For waves propagating along the x-axis in the observers frame, the entropy wave propagates with the fluid velocity: $\lambda_0 = v_x$. The eigenvalues of the two Alfvén waves are given by

$$\lambda_A^{\pm} = (u^x \sqrt{w_{\rm tot}} \pm b^x)/(u^0 \sqrt{w_{\rm tot}} \pm b^0) \ . \tag{25}$$

In our numerical scheme, however, we are interested in the eigenvalue with the largest absolute value for a given state (i.e. one of the fast magnetosonic waves) and unfortunately in RMHD there is no simple analytical expression for the magnetosonic eigenvalues. The eigenvalues $\lambda_{F,S}^{\pm}$ are the roots of the following quartic equation:

$$\begin{aligned} w(e_p' - 1)(u^0\lambda - u^x)^4 \\ - (1-\lambda^2)\left[(w + e_p' \, |b|^2)(u^0\lambda - u^x)^2 - (b^0\lambda - b^x)^2\right] = 0 \ , \end{aligned} \tag{26}$$

where $e_p' = (\partial e/\partial p)_s = c_s^{-2}$, with $c_s = (\gamma p/w)^{1/2}$ the gas dynamic sound speed. Rewriting the left hand side yields a simple fourth order polynomial in λ, but the exact analytical solution for its roots is cumbersome and inefficient to calculate numerically in the code. There is an extra complication: when the fluid velocity approaches the speed of light, the eigenvalues all tend to unity and lie very close together. This is a notoriously difficult case for root finding routines, so we transform to a new variable $\mu \equiv 1/(1-\lambda)$ and multiply the resulting equation by μ^4 resulting in a fourth order polynomial equation for μ. The roots of this equation are well separated (for $\lambda \to 1$ we have $\mu \to \infty$) and can be found using a root finding technique. In our code we employ Laguerre's method [7] for polynomials.

3 The AMRVAC Code

The Versatile Advection Code (VAC, see [8]) is a finite volume based numerical code to solve a system of conservation laws on a fixed computational grid. Recently, the code AMRVAC (Adaptive Mesh Refinement VAC) has been developed to extend the capabilities of VAC to calculations with dynamical and automatic grid refinement [1, 2]. The refinement method is summarized in Sec. 3.1. Due to the use of LASY syntax (Loop Annotated Syntax, see [9]) the code can easily be configured to run in 1D, 2D or 3D, and with one, two or three components for vector quantities. In 1D and 2D grids with cylindrical and spherical symmetry are selectable. Available physics modules are ideal hydrodynamics, ideal and resistive magnetohydrodynamics, and, as described here, also relativistic hydro- and magnetohydrodynamics.

The scheme we use for this work is a Lax–Friedrich type Total Variation Diminishing (TVD) scheme called TVDLF. The finite volume discretization of the conservation law (19) is

$$U_i^{n+1} = U_i^n - \frac{\Delta t}{\Delta x}(f_{i+1/2}^n - f_{i-1/2}^n) \,, \tag{27}$$

where U_i^n is the cell average value of the conserved variable U at the discrete time t^n for the i-th mesh cell with interfaces indicated by $i \pm 1/2$. The numerical fluxes are

$$f_{i+1/2}^n = \tfrac{1}{2}\left(F(U_{i+1/2}^L) + F(U_{i+1/2}^R) - c_{\max}\left[U_{i+1/2}^R - U_{i+1/2}^L\right]\right) \,, \tag{28}$$

where the maximum propagation speed is $c_{\max} = \max\left(\left|\lambda_{\max}(U^L)\right|, \left|\lambda_{\max}(U^L)\right|\right)$ and the states left and right of the interface are

$$U_{i+1/2}^L = U_i^n + \tfrac{1}{2}\Delta\bar{U}_i^n \,, \qquad U_{i+1/2}^R = U_{i+1}^n - \tfrac{1}{2}\Delta\bar{U}_{i+1}^n \,. \tag{29}$$

In the work presented here we use *minmod* limited slopes $\Delta\bar{U}_i^n$. Time integration is done using an explicit second order predictor-corrector scheme.

In 2D and 3D MHD calculations various schemes are selectable to ensure that $\nabla\cdot\boldsymbol{B} = 0$ is preserved during the calculation (See [2] for details). Although most of these schemes are straightforwardly adaptable to the relativistic case, we did not yet perform runs testing their results for RMHD. The simulations shown in this paper are therefore without any scheme to control $\nabla\cdot\boldsymbol{B}$ errors in the calculations.

3.1 AMR Strategy

Our AMR implementation closely follows the original algorithm in [10] for creating a properly nested hierarchy of 'optimally fitted' grids. An important difference is that during the automated creation of 'rectangular' grids, we algorithmically exclude the formation of overlapping grids at the same nesting level and enforce a minimal efficiency of each individual new grid. This efficiency is determined as the ratio of cells identified for refinement to the total number of cells contained within the rectangle. Specifically, once an arbitrary number of cells is flagged for refinement, one subsequently surrounds each cell with a user-set zone of buffer cells (connected to the temporal frequency with which a full regridding cycle is activated to ensure consistency with the CFL constraint); which are then processed into non-overlapping rectangles by a sequence of mergers and bisections. Note that this approach differs from the Berger and Rigoutsous [11] algorithm exploiting edge detection from pattern recognition techniques. Similarly though, our AMR implementation creates optimally fitted, but very different sized higher level grids. Parallelization is done using `OpenMP` which was shown to work effectively on up to several tens of processors on `ccNUMA` architectures [1, 12, 2]. The parallelism is exploited over the grids per refinement level, and works well when the number of grids on each grid level exceeds the number of processors in use.

The refinement criterion is a variant of the Richardson-type error estimation procedure from Berger and Collela [13], which is generally applicable to any system of equations and integration method used. Needed are two solution vectors $\boldsymbol{U}_l^{n-1}$ and $\boldsymbol{U}_l^n$ on level l, separated in time by the corresponding Δt_l^{n-1}. The error is estimated as follows:

- coarsen the $\boldsymbol{U}_l^{n-1}$ spatially by a factor of 2 to obtain $\boldsymbol{U}_{2\Delta x_l}^{n-1}$;
- advance $\boldsymbol{U}_{2\Delta x_l}^{n-1}$ using $2\Delta t_l^{n-1}$ to $\boldsymbol{U}_{\mathrm{c}}^{n+1}$;
- advance $\boldsymbol{U}_l^n$ with Δt_l^{n-1} to $\boldsymbol{U}_{\mathrm{f}}^{n+1}$;
- spatially coarsen (average) $\boldsymbol{U}_{\mathrm{f}}^{n+1}$ to $\overline{U_{\mathrm{f}}}$
- using the solutions $\boldsymbol{U}_{\mathrm{c}}^{n+1}$, $\boldsymbol{U}_{\mathrm{f}}^{n+1}$, and $\overline{U_{\mathrm{f}}}$ all corresponding to time $t = t_l^{n-1} + 2\Delta t_l^{n-1}$, flag for refinement on the basis of a selection of weighted tolerance criteria.

The latter typically compares selected components of the conserved variables, problem-dependently chosen with mutual weighting factors. One then flags for refinement when a critical tolerance level ϵ_{tol} is exceeded. It is possible to extend the refinement criteria with user-forced refinement or derefinement, or exploit primitive or auxiliary variables (like the Lorentz factor for the relativistic simulations discussed here) in the flagging criterion. The need for additionally exploiting uncoarsened data $\boldsymbol{U}_{\mathrm{f}}^{n+1}$ is advocated by Bell et al. [14]. As a result, where the criterion is fulfilled, a multitude of 2^D level l cells are flagged, for a D-dimensional problem.

We point out that in AMRVAC, we can already allow for a level-dependent choice of the discretization scheme employed. This is a first step toward full

Adaptive Mesh and Algorithm Refinement (AMAR), introduced by Garcia et al. [15], who coupled a continuum description with a particle method on the finest level of the AMR hierarchy. The possibility to couple different physics modules across the various grid levels is due to the fact that the only communication between different level solutions is through (i) the update process that is needed to keep the different level solutions consistent and to restore global conservation and (ii) the filling of 'ghost' cells as used for imposing boundary conditions. It is conceivable that once a suitable mapping of the fluxes used in the update process for non-relativistic versus fully relativistic simulations is properly implemented, one could solve for (M)HD flow problems where both non-relativistic versus ultra-relativistic flow regions are essential ingredients. On the various grid levels, one would then solve the corresponding HD, MHD, RHD, or RMHD equations depending on the locally occurring flow velocities and magnetic field strengths.

4 Results

With the methods outlined in the previous sections various test runs were performed.For all runs we took $\gamma = 4/3$ for the adiabatic constant.

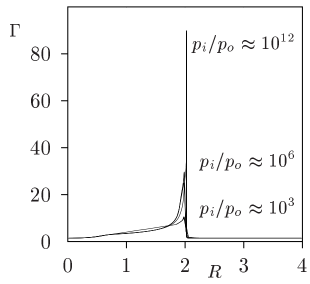

Fig. 1. The Lorentz factor Γ versus radius for spherical explosions with different initial pressure ratios. A base grid of 50 cells and four refinement levels with a refinement factor of 4 on each level was used, resulting in an effective resolution of 128 000 cells.

First a simple 1D spherical RHD explosion was set up by putting a high pressure in a small region around the origin and simulating the resulting expansion. At $t = 0$ we take $(\rho, v_r, p) = (1.0, 0, p_i/p_o)$ for $0 < r \leq 0.1$ and $(\rho, v_r, p) = (1.0, 0, p_o)$ for $0.1 < r \leq 4.0$, where $p_o = 0.001$ in all cases. The outgoing blast wave sweeps up matter in a thin and dense shell. This shell lies between the forward shock and a contact discontinuity, and due to Lorentz contraction its thickness, and thus the separation between the two discontinuities, is inversely proportional to the Lorentz factor of the blast wave. By increasing the initial pressure ratio p_i/p_o we increase the Lorentz factor of the resulting blast wave, as can be seen in Fig. 1. The extreme pressure contrast and thinness of the shock wave require locally very high grid resolutions, which shows that AMR is indispensable in relativistic simulations.

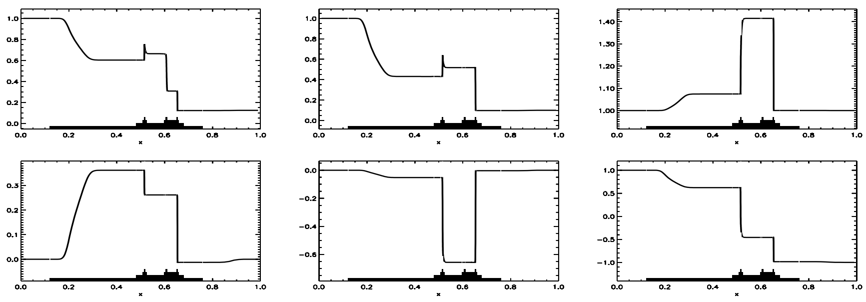

Fig. 2. Relativistic analog of the Brio–Wu shock tube test. The panels, from left to right and from top to bottom, show: density, pressure, Lorentz factor, x-velocity, y-velocity and perpendicular magnetic field B_y.

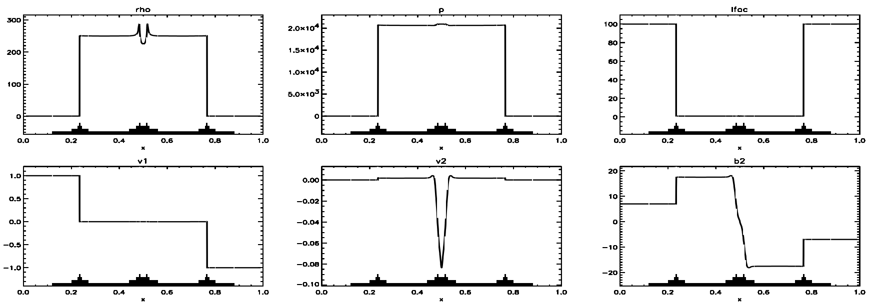

Fig. 3. Flow collision test; ultra-relativistic flows ($\Gamma = 100$) collide at $x = 0.5$. Panels are the same as Fig. 2.

Next we performed two 1D RMHD shock-tube tests, the first is the relativistic analog of the Brio–Wu shock tube test, see Fig. 2. Initial conditions are $(\rho, v_x, v_y, p, B_x, B_y) = (1.0, 0, 0, 1.0, 0.5, 1.0)$ for $x \leq 0.5$ and $(0.125, 0, 0, 0.1, 0.5, -1.0)$ for $x > 0.5$. The second (Fig. 3) is a flow collision problem with two $\Gamma = 100$ flows colliding at $x = 0.5$. Initial conditions are $(\rho, v_x, v_y, p, B_x, B_y) = (1.0, \pm 0.99995, 0, 0.1, 10.0, \pm 7.0)$ for $x \lessgtr 0.5$. In both cases the AMR algorithm accurately tracks all shocks and waves (4 levels with a refinement ratio of 4 on each level, the base level consists of 50 cells). In the flow collision problem a noticeable 'wall heating' error around $x = 0.5$ occurs, but otherwise the code handles the extreme shocks satisfactory.

A more astrophysically relevant simulation is the axisymmetric 2D RHD relativistic jet shown in Fig. 4. A jet with radius $r_0 = 1.0$, density $\rho = 0.1$ and pressure $p = 0.01$ is injected with $v_z = 0.99$ ($\Gamma \approx 7$) into a homogeneous background with $\rho = 10.0$ and $p = 0.01$. The domain of the calculation is $0 < r < 8, 0 < z < 20$ with a base grid of 80×120. Three additional grid levels were used with a refinement factor of two, giving an effective resolution of 640×1600.

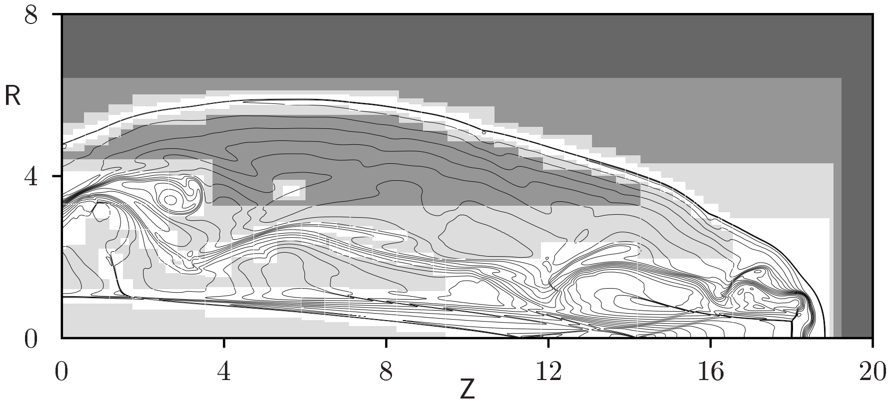

Fig. 4. Axisymmetric RHD jet with $\Gamma \approx 7$. Equidistant contours of $\log \rho$ are shown and the 4-level grid structure is indicated by grayscales.

Finally the relativistic extension of the 2D MHD rotor test from [6] is shown in Fig. 5. An initially rotating disk of dense plasma is embedded in a homogeneous magnetic field $\boldsymbol{B} = 1.0\boldsymbol{e}_x$ ($(\rho, v_x, v_y, p) = (10.0, -\alpha y, \alpha x, 1.0)$ for $(x^2 + y^2)^{1/2} < 0.1$, where $\alpha = 9.95$; the background is $(\rho, v_x, v_y, p) = (1.0, 0, 0, 1.0)$). The maximum Lorentz factor is about 10. The disk is decelerated by the winding of the magnetic field lines, and the plasma is flung outward in and oblong shell. Strong shocks and torsional Alfvén waves are generated. The results of this complex 2D RMHD problem agree quite well with the results published in [6].

5 Conclusions

The multi-dimensional grid adaptive code AMRVAC is extended with relativistic hydrodynamics and relativistic magnetohydrodynamic modules. The code performed quite well on all test problems, the AMR algorithm speeds up the calculations presented here so that they could easily be performed on a single desktop processor. Extension toward larger resolutions and higher Lorentz factors is expected to be straightforward as AMRVAC has been shown to perform well on larger parallel computers [12]. To asses the reliability and

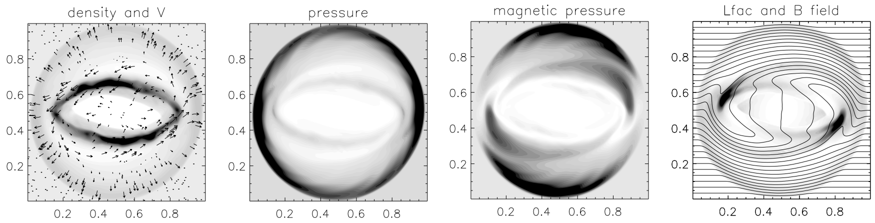

Fig. 5. RMHD rotor simulation at $t = 0.4$. Three grid levels with a refinement factor 2, effective resolution is 400×400 cells.

accuracy of the multidimensional ultra-relativistic calculations it is however desirable to compare results obtained by different R(M)HD solvers in a more quantitative study. Such a validation is essential to get a reliable understanding of the astrophysical objects that we try to model with these computations.

Acknowledgments

This work is part of the Computational Science project "Rapid Changes in Complex Flows" of the Dutch Organization for Scientific Research NWO.

References

1. M. Nool and R. Keppens, Comput. Methods Appl. Math., **2** 92 (2002).
2. R. Keppens, M. Nool, G. Tóth, and J.P. Goedbloed, Comput. Phys. Commun., **153** 317 (2003).
3. L. D. Landau and E. M. Lifshitz: Fluid mechanics (Pergamon Press, 1959).
4. A. V. Koldoba, O. A. Kuznetsov, and G. V. Ustyugova, Mon. Not. Astron. Soc. **333** 932 (2002).
5. S. S. Komissarov, Mon. Not. Astron. Soc. **303** 343 (1999).
6. L. Del Zanna, N. Bucciantini, and P. Londrillo, A&A **400** 397 (2003).
7. W. H. Press, S. A. Teukolsky, W. T. Vetterling, and B. P. Flannery: Numerical recipes, 2nd ed. (Cambridge University Press, 1992).
8. G. Tóth, Astrophys. Lett. Comm. **34** 245 (1996).
9. G. Tóth, J. Comput. Phys. **138** 981 (1997).
10. M.J. Berger, SIAM J. Sci. Stat. Comput. **7** 904 (1986).
11. M.J. Berger and I. Rigoutsos, IEEE Transactions on Systems, Man and Cybernetics **21**, 1278 (1991).
12. R. Keppens and G. Tóth, Lect. Notes Comp. Science **2329** 940 (2002).
13. M.J. Berger and P. Colella, J. Comput. Phys. **82** 64 (1989).
14. J. Bell, M. Berger, J. Saltzman and M. Welcome, SIAM J. Sci. Comp. **15** 127 (1994).
15. A.L. Garcia, J.B. Bell, W.Y. Crutchfield and B.J. Alder, J. Comput. Phys. **154** 134 (1999).